Infrared Spectra of Hydrogen-Bonded Ionic Crystals: Ab Initio Study of $Mg(OH)_2$ and β-$Be(OH)_2$

Piero Ugliengo,*,† Fabien Pascale,‡ Mohammadou Mérawa,§ Pierre Labéguerie,§ Sergio Tosoni,† and Roberto Dovesi†

Dipartimento di Chimica IFM, Università di Torino, Via P. Giuria, 7. 10125 Torino, Italy, Laboratoire de Cristallographie et Modélisation des Matériaux Minéraux et Biologiques (LCM3B) UMR−CNRS 7036, Université Henri Poincaré Nancy I BP 239, Boulevard des Aiguillettes F54506 Vandoeuvre-les-Nancy Cedex, France, and Laboratoire de Chimie Théorique et de Physico-Chimie Moléculaire, UMR 5624, FR 'IPREM' 2606, IFR−rue Jules Ferry, F-64000 Pau, France

Received: June 9, 2004; In Final Form: June 30, 2004

Ab initio periodic calculations have been performed with the CRYSTAL code, which is based on Gaussian basis sets, to investigate the structure and OH vibrational features (both harmonic and anharmonic) of $Mg(OH)_2$ and β-$Be(OH)_2$ crystals, which represent two extreme situations in which the OH group can be involved. In the latter, it participates in H-bonds of intermediate strength, whereas, in the former, it is essentially free. Hartree−Fock (HF), local density (LDA), gradient-corrected (PW91), and hybrid (B3LYP) density functionals have been used and the results compared with experiment. For $Mg(OH)_2$, the B3LYP OH frequencies are in very good agreement with experiment, whereas, for β-$Be(OH)_2$, they are $\sim$100 cm^{-1} too low. LDA grossly underestimates the OH frequency (330 and 800 cm^{-1} for $Mg(OH)_2$ and β-$Be(OH)_2$, respectively), and PW91 moderately does (170 and 400 cm^{-1}, respectively).

1. Introduction

The introduction of accurate functionals has made density functional theory a valid alternative to the most traditional (and also much more computationally demanding) post-Hartree−Fock methods for taking electron correlation into account. Although many studies have been devoted in recent years to establishing the accuracy of the available functionals in predicting the structures and vibrational features of molecules,[1] far less is known when crystalline materials are involved. Most of the commonly adopted computer codes for treating crystals at the ab initio level are based on a plane wave basis set combined with effective pseudopotentials to treat core electrons. Usually the PW91 gradient-corrected functional[2−5] is adopted for the vast majority of the calculations. Because of the difficulty of dealing with Hartree−Fock exchange, plane wave codes cannot use hybrid functionals such as the one proposed by Becke,[6] where a given fraction of exact Hartree−Fock exchange is embedded in the definition of the hybrid (B3LYP) functional. For molecules, the introduction of a fraction of exact exchange has been shown to be beneficial for a better description of geometries, frequencies, and reaction barriers.[1] Besides the modeling of molecular properties, it is of great relevance to model with a high degree of accuracy also molecular aggregates, held by relatively weak intermolecular interactions. This is of paramount importance for the understanding of molecular recognition, drug design, and crystal engineering. Among intermolecular interactions, the H-bond assumes a prominent role because it is ubiquitous in biochemistry and is a main driving force in holding molecular crystals in place.

When a system sports H-bond forces, the hydrogen donor bond gets elongated by the intermolecular interaction and its force constant is reduced, as is the associated vibrational stretching frequency (bathochromic shift). Furthermore, the motion of the proton becomes quite anharmonic because of the attraction exerted by the H-acceptor. The bathochromic shift is an important fingerprint of the H-bond, and a lot of experimental work is devoted to measuring its value because its entity is a function of the H-bond strength. This is also true when the H-bond occurs at the surface of crystalline inorganic materials such as silica[7] or in the interior of acidic zeolites in which the H-bond is the first step of further reactive steps. From a computational viewpoint, it is important to establish the performance of density functional theory (DFT) in that respect. Information concerning the performance of various functionals in computing the vibrational features of H-bonded systems is scarce. Some of us have dealt with molecular H-bonded complexes in the past,[8] and the present work is an extension to semi-ionic crystals, namely, brucite ($Mg(OH)_2$), as a prototype of a crystal with OH groups free from any H-bonding interactions, and β-$Be(OH)_2$, where an infinite network of H-bonds exists. The CRYSTAL code has been used because it allows one to perform calculations at the B3LYP level as well as at the Hartree−Fock (HF) level and to adopt a variety of local and gradient-corrected density functionals. The code expands the crystalline orbitals in terms of localized Gaussian basis sets, allowing for direct comparison with molecular results. The study takes profit of the new feature recently encoded in the CRYSTAL code, that is, the ability to compute the full set of harmonic frequencies for a crystalline system by diagonalization of the ab initio force constant matrix.[9] The harmonic OH frequencies have also been improved by computing the anhar-

† Università di Torino.
‡ Laboratoire de Cristallographie et Modélisation des Matériaux Minéraux et Biologiques (LCM3B).
§ Laboratoire de Chimie Théorique et de Physico-Chimie Moléculaire.

10.1021/jp047514v CCC: $27.50
Published on Web 08/12/2004

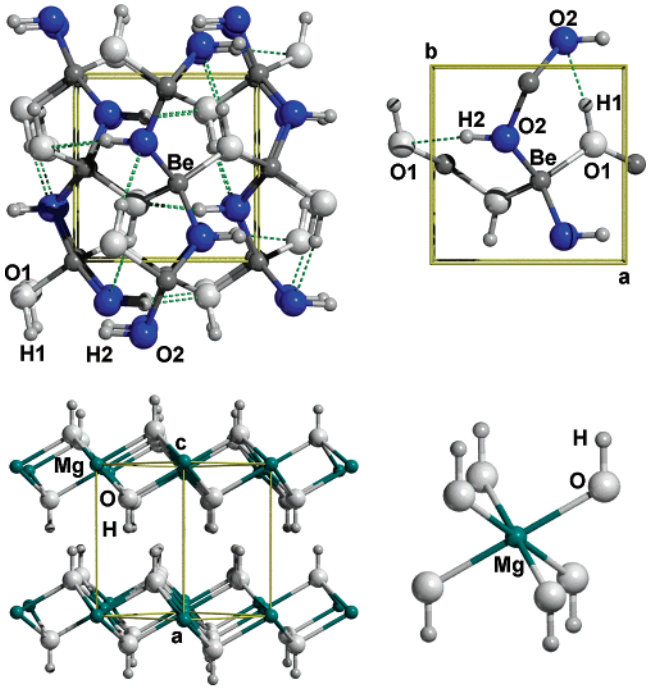

Figure 1. (top) Portion of the β-$Be(OH)_2$ crystal viewed normal to the (001) plane and local coordination of the Be ion with the standard numbering (ref 13). (bottom) Portion of the $Mg(OH)_2$ crystal viewed normal to the (110) plane and local coordination of the Mg ion.

monic contribution so that a more straightforward comparison with experiment is possible.

2. Computational Details

2.1. Structural Models. Brucite ($Mg(OH)_2$) is a highly symmetric layered structure (space group, $P\bar{3}m1$) with a relatively small (five atoms per cell) unit cell.[10] The cation is 6-fold-coordinated (see Figure 1, bottom). The OH groups are vertical, with the shortest H···H interlayer and intralayer distances at 1.97 and 3.15 Å, respectively. The interaction, if any, among the OH groups is thus very weak, so that brucite is a prototype of a crystal with OH groups free from any H-bonding interactions.

β-$Be(OH)_2$ crystallizes in the acentric orthorhombic space group $P2_12_12_1$ with four formula units in the unit cell; for its structure, we refer to a neutron diffraction study[11] and to a very recent extension of that study[12] in which the dependence of the structure on the temperature has been studied for $T = 294$, 254, 50, and 5 K, the latter being ideally suited for comparison with the theoretical results. The crystal structure has two crystallographically different OH groups, as shown in Figure 1; both OH groups are involved in a complex infinite network of H-bonds. β-$Be(OH)_2$ is adopted here as a prototype of a crystal in which, at variance with respect to brucite, the OH groups are involved in H-bonding interactions of intermediate strength because of the high polarization power of the Be cation.[13]

2.2. Methods. All calculations have been performed with a development version of the CRYSTAL program[14] running on standard Linux PCs. For the geometry optimization, both unit cell parameters and fractional atomic coordinates have been relaxed using a specific CRYSTAL driver.[15] The unit cell parameters are fixed and the internal coordinates are relaxed by means of the analytical energy gradients[16,17] toward the equilibrium structure, using a modified conjugate gradient algorithm as proposed by Schlegel.[18] Convergence is tested on the root mean square (rms) and on the absolute value of the largest component of both the gradients and the estimated nuclear displacements. The thresholds for the maximum and the rms forces and the maximum and the rms atomic displacements on all atoms have been set to (in atomic units) 0.000 45, 0.000 30 and 0.001 80, 0.001 20, respectively. The cell parameters are then optimized by evaluating numerically the relative energy gradients; the whole process is reiterated until the above convergence criteria are satisfied. Four Hamiltonians have been adopted: Hartree−Fock (HF); local density functional (LDA) based on Dirac exchange[19] and the Vosko−Wilk−Nusair[20] correlation contribution; Perdew−Wang (PW91) gradient-corrected exchange and correlation functional;[2−5] and Becke's three-parameter (B3LYP) hybrid exchange functional[6] in combination with the gradient-corrected correlation functional of Lee, Yang, and Parr.[21]

In the CRYSTAL code, crystalline orbitals are expanded in terms of a Gaussian type basis set; for the present case, the following Gaussian type orbitals have been used (the α exponents of the most diffuse shells are given below, in $bohr^{-2}$). (i) Mg: 8-511G* basis set[22,23] ($\alpha_{sp} = 0.68$ and 0.28); ($\alpha_d = 0.6$). (ii) Be: 5-11G basis set developed for the BeO crystal[24,25] ($\alpha_{sp} = 0.629$). (iii) O: 8-411G* basis set[22,23] ($\alpha_{sp} = 0.495$ and 0.190); ($\alpha_d = 0.8$). (iv) H: 2-11G* basis set[26] ($\alpha_{sp} = 0.12$); ($\alpha_p = 0.9$). For $Mg(OH)_2$ and β-$Be(OH)_2$, the number of reciprocal lattice points (k-points) at which the Hamiltonian matrix has been diagonalized is 65 and 64, corresponding to shrinking[14] factors of $S = 8$ and 6, respectively. Default values of the tolerances that control the Coulomb and exchange series have been adopted.[14] For DFT, the exchange-correlation functional is integrated numerically on a grid of points. Integration over radial and angular coordinates is performed through Gauss−Legendre and Lebedev schemes, respectively. A pruned grid consisting of 75 radial points and 5 subintervals with (86, 194, 350, 974, and 350) angular points has been used for all calculations. This grid setting gives about 53 000 and 110 000 integration points per unit cell for $Mg(OH)_2$ and β-$Be(OH)_2$, respectively, which produces an error of 2.0×10^{-5} and 1.7×10^{-5} electrons, respectively, in the total number of electrons per cell, obtained by integrating the electron density.

The phonon frequencies in a periodic system and within the harmonic approximation are obtained by diagonalizing the central zone ($k = 0$) mass weighted Hessian matrix:

$$W_{ij}(k=0) = \sum_G \frac{H_{ij}^{0G}}{\sqrt{M_i M_j}}$$

where H_{ij}^{0G} is the potential second derivative, at equilibrium, with respect to the position of atom i in cell 0 and atom j in cell G. In CRYSTAL, energy first derivatives with respect to the atomic positions, $v_j = \partial V/\partial u_j$, are calculated analytically for all u_j coordinates, while second derivatives at $u = 0$ are calculated numerically using a three-point formula:

$$\left[\frac{\partial v_j}{\partial u_i}\right]_0 \approx \frac{v_j(0, \ldots, u_i, \ldots) - v_j(0, \ldots, -u_i, \ldots)}{2u_i}$$

In this paper, we have adopted a step of 0.001 Å for the numerical differentiation. More details on this topic can be found in ref 9.

The anharmonicity of the OH stretching mode has been computed following the same procedure recently adopted by some of us.[26,27] It consists of the following steps: (i) the OH distance is treated as a pure normal coordinate decoupled with respect to all other modes; (ii) the total energy of the system is

TABLE 1: Experimental and Computed Cell Parameters (in Å), Main Geometrical Features (Distances in Å, Angles in Degrees), and Cell Volumes, V_C (in Å^3), of $Mg(OH)_2$ and β-$Be(OH)_2$

$Mg(OH)_2$					
	experimental[a]	HF	LDA	PW91	B3LYP
a	3.150	3.148	3.099	3.179	3.167
c	4.770	5.263	4.413	4.717	4.854
V_C	41.0	45.2	36.7	41.3	42.2
Mg−O	2.100	2.093	2.067	2.111	2.104
O−H	0.958	0.940	0.982	0.972	0.962
Mg−O−H	120.0	119.7	120.1	119.6	119.6
H···H(interlayer)	1.969	2.239	1.829	1.960	2.016
H···H(intralayer)	4.409	4.352	4.413	4.428	4.402
β-$Be(OH)_2$					
	experimental[b]	HF	LDA	PW91	B3LYP
a	4.533	4.651	4.291	4.474	4.528
b	4.625	4.714	4.487	4.631	4.653
c	7.038	7.061	6.857	6.997	7.035
V_C	147.6	154.8	132.0	145.0	148.2
⟨Be−O⟩	1.632	1.633	1.624	1.648	1.643
O1−H1	0.956	0.946	1.028	0.996	0.977
O2−H2	0.952	0.947	1.032	0.999	0.979
H1···O2	2.007	2.182	1.560	1.781	1.898
H2···O1	1.993	2.158	1.547	1.758	1.874
O1−H1···O2	148.1	144.8	156.6	153.7	151.2
O2−H2···O1	158.8	155.4	168.9	165.3	162.5

[a] Reference 10. [b] Reference 11.

calculated for a set of OH values around equilibrium (−0.2/+0.3 Å), and a sixth-order polynomial fit is used to interpolate these points; (iii) the one-dimensional nuclear Schrödinger equation (NSE) is solved following the algorithm proposed by Lindberg[28] and coded in the program ANHARM[29] that produces the three lowest eigenvalues, E_0, E_1, and E_2, that are then used to compute $\omega_{01} = E_1 - E_0$, $\omega_{02} = E_2 - E_0$, and $\omega_e x_e = (2\omega_{01} - \omega_{02})/2$. For $Mg(OH)_2$, two OH stretching modes are possible; the anharmonic analysis has been limited to the symmetric stretching only. For β-$Be(OH)_2$, eight OH stretching modes are possible. Only two OH modes are of A_1 symmetry, separately involving mainly the family of OH1 and OH2 bonds, respectively. The anharmonic study has been performed only for these two modes.

3. Results and Discussion

3.1. Geometries of $Mg(OH)_2$ and β-$Be(OH)_2$. The optimized geometry of $Mg(OH)_2$ is shown in Table 1 for the adopted Hamiltonians. Although the cell parameter *a* is well described by all Hamiltonians, the cell parameter *c*, which controls the interlayer separation, is overestimated by HF (10%) and B3LYP (<2%), underestimated by LDA (8%), and in very good agreement by PW91 (1%). This high variability of the *c* parameter is due to the very weak interaction between layers, which is difficult to be accounted for because large *c* errors imply small energy differences; besides that, also, basis set superposition error (BSSE) may play a relevant role in the location of the very shallow minimum. The OH bond distance is underestimated by HF and overestimated by all DFT Hamiltonians in the order LDA > PW91 > B3LYP. The interlayer H···H distance depends directly on the *c* parameter, so that the same comments as those above also apply here.

The optimized structure of β-$Be(OH)_2$ is reported in Table 1. PW91 and B3LYP perform very well, the latter being marginally better than the former, whereas HF and LDA overestimate and underestimate the cell volume. For H-bonded structures such as β-$Be(OH)_2$, the size of the unit cell is determined by the intermolecular H···O distances. Table 1 shows that HF and LDA grossly overestimate and underestimate them, in agreement with the cell volume values. Also, PW91 underestimates all H···O distances as does B3LYP, even if the latter gives values in better agreement with experiment than the former. As expected, OH bond lengths anticorrelate with the H···O values, because a short H···O distance means a strong H-bond which, in turn, causes OH bond elongation. LDA behaves particularly badly in that respect, the OH bond lengths being significantly longer than 1.0 Å. New geometrical results[12] show that both O1−H1 and O2−H2 lengthen from 0.956 and 0.952 Å (data in Table 1 measured at 298 K) to 0.961 and 0.973 Å, respectively, obtained at temperatures as low as 5 K. Data at low *T* are in better agreement with the B3LYP results, which also predicts the O2−H2 bond length to be slightly longer than O1−H1. Also, the angles around the O−H···O moiety are described better by B3LYP than by the other Hamiltonians.

TABLE 2: Experimental and Computed OH Vibrational Features of $Mg(OH)_2$[a]

mode	experiment[b]	HF	LDA	PW91	B3LYP
ω_h (Raman)		4220	3558	3691	3847
ω_e (Raman)		4219	3550	3680	3843
ω_{01} (Raman)	3654	4070	3325	3480	3663
ω_{02} (Raman)	7157	7990	6424	6760	7148
$\omega_e x_e$ (Raman)	98	75	113	100	90
ω_h (IR)		4220	3642	3739	3873
ω_{01} (IR)	3698	4070[c]	3410[c]	3536[c]	3693[c]
Δ_h		0	84	48	25
Δ_{01}	44	0	85	56	30

[a] ω_h is the harmonic OH frequency from the dynamical second derivative matrix; ω_e, ω_{01}, ω_{02}, and $\omega_e x_e$ are respectively the harmonic, the fundamental, the first overtone, and the anharmonicity constant of the OH mode computed by solving the 1D NSE; and Δ_h and Δ_{01} are the splitting between the Raman and IR modes computed using the harmonic and fundamental OH frequencies, respectively. All data are in inverted centimeters. [b] Reference 30 [c] Computed by correcting the harmonic ω_h (IR) value with the same $\omega_e x_e$ value that was computed for the ω_{01} (Raman) value.

3.2. Vibrational OH Frequencies. $Mg(OH)_2$ has two symmetry related OH groups within the same layer, well far apart from each other (more than 4.0 Å, see Table 1), linked to the same Mg ion. The interlayer H···H distance is much smaller than the intralayer one (around 2.0 Å, see Table 1 and Figure 1, bottom), so that it is expected that the vibrational splitting between the symmetric and antisymmetric OH stretching modes is to a large part due to the interlayer coupling. The symmetric mode is Raman active, and has a lower frequency, while the antisymmetric mode is IR active. Experimentally,[30] these two frequencies differ by 44 cm^{-1} (see Table 2). The experimental $\omega_e x_e$ constant was obtained by Weckler and Lutz[30] from the ω_{01} and ω_{02} values using the equations reported in the Methods section, for the IR mode only. Actually, the attribution of the frequency at 7157 cm^{-1} to the IR OH overtone, rather than to a combination of the IR and Raman fundamental frequencies as proposed by Mitra[31] and other authors,[32,33] leaves some marginal doubts about the proposed $\omega_e x_e$ values.

Regarding the calculations, the NSE has been solved for the symmetric stretching mode, moving in phase the two symmetry related hydrogen atoms. The computed anharmonic constant, $\omega_e x_e$, has been used for correcting also the harmonic ω_h frequency of the antisymmetric (IR active) mode computed by diagonalizing the fully coupled force constants matrix; the same $\omega_e x_e$ value is then attributed to both modes. HF overestimated the ω_{01} value, as expected, whereas LDA grossly underestimated it. PW91 marginally improves over LDA, whereas B3LYP performs very well, its prediction being only 9 cm^{-1} higher than

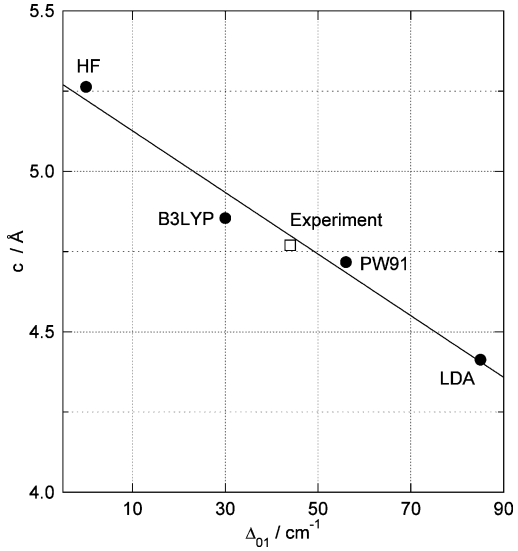

Figure 2. Correlation between the cell parameter *c* and the vibrational Raman-IR Δ_{01} splitting of the two OH stretching modes of $Mg(OH)_2$ obtained with the various Hamiltonians.

experiment. The IR mode shows a similar trend, the B3LYP datum being 5 cm^{-1} lower than experiment. Remarkably, B3LYP is accurate also in the overtone region where all other methods give a too flat potential energy. The calculated B3LYP Raman anharmonicity constant is $\sim$10 cm^{-1} smaller than the one estimated from experiment. It must be noticed that also the anharmonicity constants calculated by Engstrom[34] and by Berglund,[35] for various hydroxides including $Mg(OH)_2$, by using the H $\rightarrow$ D isotopical substitution data for the ω_{01} frequency, rather than the ω_{02} overtone data, provide anharmonic constants lower than the ones evaluated by Weckler.[30]

The B3LYP Δ_{01} computed Raman-IR splitting of 30 cm^{-1} is smaller than the experimental value, while PW91 slightly overestimated it (56 cm^{-1}) and LDA overestimated it even more so (85 cm^{-1}), whereas HF was unable to give any difference. The Δ_{01} splitting correlates with the interlayer separation (that coincides with the cell parameter *c*), as shown in Figure 2 (data in Table 1). In that respect, we can conclude that the OH Raman-IR splitting is a function of the intermolecular interaction between layers.

The β-$Be(OH)_2$ full harmonic set of frequencies has been computed only at the B3LYP level, due to the relatively high computational cost. As described in the section devoted to structural models, β-$Be(OH)_2$ has two families of OH bonds, giving rise to eight OH stretching modes at Γ point. Table 3 gives the B3LYP OH harmonic frequencies: the modes are all both Raman and IR active, with the exception of the two totally symmetric modes which are Raman active only. Visual analysis of the modes and recourse to the potential energy distribution (PED) analysis of the normal modes (available in the CRYSTAL03 code) reveal that the eight modes can be divided into two blocks, each involving mainly one of the two OH*i* stretching modes. Figure 3 shows the detailed analysis of the displacements associated with each normal mode; it shows that (i) within the OH2 block, in the B_3 and A_1 modes, there is some marginal participation of the OH1 groups too, whereas the B_1 and B_2 modes are almost pure OH2 stretchings and (ii) within the OH1 block, B_1 and B_2 modes are pure OH1 stretchings, whereas, in the A_1 and B_3 modes, some coupling with OH2 groups is active.

To fully decouple the two family modes, isotopical substitution (H $\rightarrow$ D) has been used in various ways; the results are reported in Table 3. The first column contains data already reported in Figure 3. The effect of deuteration of all hydrogen atoms of the OH1 family on the stretching frequencies of the OH2 modes is shown in column 2. As expected from inspection of Figure 3, only the B_3 and A_1 OH2 modes are affected by deuteration (shift of 31 and 24 cm^{-1}, respectively), whereas the other two move by 0 and 2 cm^{-1}, respectively. The same effect is shown in column 3 of Table 3, in which, this time, selective deuteration of OH2 bonds leaves unaltered the B_1 and B_2 OH1 modes, whereas the A_1 and B_3 modes shift by 21 and 27 cm^{-1}, respectively (compare the last two rows of columns 1 and 3, respectively). The last column of Table 3 gives the computed spectra for a fully deuterated crystal. The development version of the CRYSTAL03 code permits the calculation of infrared intensities[36] (Raman intensities not yet available). Table 3 shows that, of the six symmetry allowed bands, the predicted IR spectra only have four bands of significant intensity.

Experimentally,[13] four OH modes have been detected in IR spectra (3407, 3440, 3458, and 3482 cm^{-1}) and three in the Raman spectra (3413, 3464, and 3476 cm^{-1}). The spread of the OH band is $\sim$80 cm^{-1}, which should be compared with the B3LYP value of 96 cm^{-1} computed using the harmonic frequencies. Experimentally,[13] partial deuteration has also been used in order to decouple the OH modes. IR modes are found at (2542, 2549, 2565, and 2571 cm^{-1}) and the Raman ones at (2544, 2551, 2566, and 2568 cm^{-1}). A more thorough analysis of the experimental data[13] for isotopically dilute samples has allowed us to assign the OH1 stretching mode a value of 2566 cm^{-1} and the OH2 stretching mode a value of 2551 cm^{-1}. With respect to these two modes, a complete anharmonic analysis has been carried out for the whole set of Hamiltonians by the following procedure. For the two OH1 and OH2 totally symmetric modes, the protons not belonging to the considered family (either OH1 or OH2) are kept fixed during either the OH1 or OH2 elongation. The results are collected in Table 4

TABLE 3: Harmonic B3LYP OH Frequencies of β-$Be(OH)_2$[a]

symmetry	$(OH2)_4$	IR intens	$(OH2)_4$	IR intens	$(OD2)_4$	IR intens	$(OD2)_4$	IR intens
B_3	3500	m	3531	vw	2579	vw	2560	m
A_1	3501		3525		2574		2561	
B_1	3536	m	3536	m	2580	m	2580	m
B_2	3541	vs	3543	vs	2588	s	2586	s
symmetry	$(OH1)_4$	IR intens	$(OD1)_4$	IR intens	$(OH1)_4$	IR intens	$(OD1)_4$	IR intens
B_1	3573	w	2607	vw	3573	w	2607	w
B_2	3575	vw	2612	vw	3574	vw	2613	vw
A_1	3585		2603		3564		2618	
B_3	3595	s	2603	s	3568	vs	2624	s

[a] Each column shows the frequencies of the two OH (OH2 and OH1) families at different deuteration regimes. The symmetry labels follow the standard notation of the 222-point-group character table. The labels for the IR intensity are the following: vw, very weak; w, weak; m, medium; s, strong; and vs, very strong. The frequencies are in inverted centimeters.

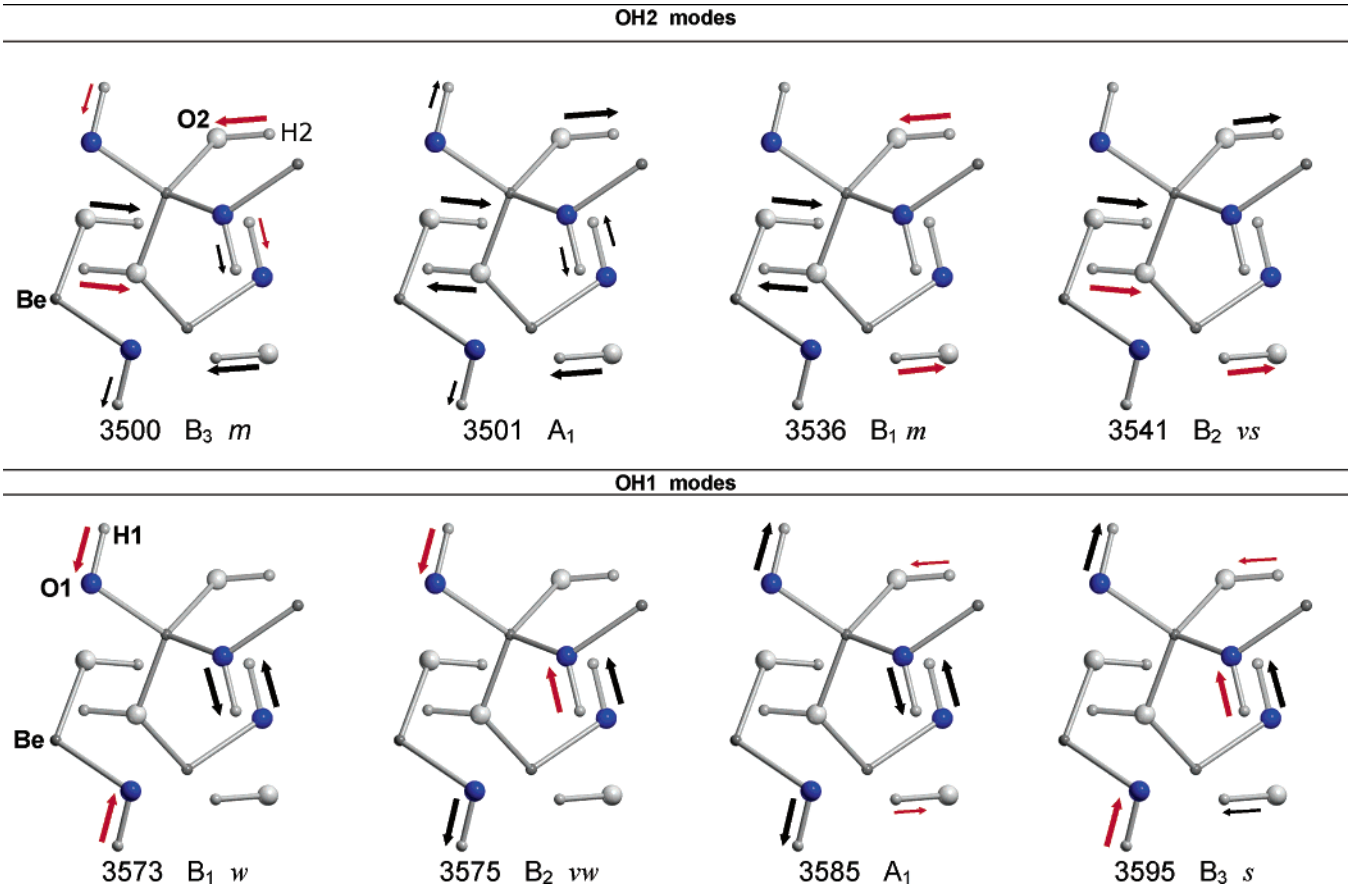

Figure 3. Schematic view of the normal modes associated to the OH stretching for the β-Be(OH)$_2$ crystal. The light and dark balls identify the OH1 and OH2 groups, respectively. The arrow size is proportional to the displacement of the involved atoms. s, vs, m, w, and vw stand for strong, very strong, medium, weak, and very weak, respectively, and refer to the IR intensity. The frequencies are in inverted centimeters.

TABLE 4: Experimental and Computed OH1 and OH2 (OD1 and OD2) Vibrational Features of β-Be(OH)$_2$[a]

OH1	experiment (OD1)	HF	LDA	PW91	B3LYP
ω_e		4100 (2985)	2705 (2018)	3266 (2377)	3570 (2595)
ω_{01}	(2566)[b]	3943 (2902)	2285 (1757)	2957 (2213)	3326 (2468)
ω_{02}		7730 (5721)	4149 (3253)	5604 (4261)	6407 (4810)
$\omega_e x_e$		78 (41)	210 (131)	155 (82)	122 (64)
δ		(+336)	(−809)	(−353)	(−98)
OH2	experiment (OD2)	HF	LDA	PW91	B3LYP
ω_e		4089 (2976)	2560 (1951)	3218 (2338)	3537 (2569)
ω_{01}	(2551)[b]	3925 (2890)	2200 (1694)	2868 (2155)	3269 (2431)
ω_{02}		7687 (5694)	4039 (3132)	5387 (4127)	6270 (4724)
$\omega_e x_e$		82 (43)	180 (129)	175 (92)	134 (69)
δ		(+339)	(−857)	(−396)	(−120)

[a] ω_e, ω_{01}, ω_{02}, and $\omega_e x_e$ are respectively the harmonic, the fundamental, the first overtone, and the anharmonicity constant of the OH (OD) mode computed by solving the 1D NSE for the two total symmetric OH stretching modes. δ is the difference between the ab initio and the experimental ω_{01} frequencies for the OD mode. All data are in inverted centimeters. [b] Reference 13.

for the cases of both OH and OD. In the same table, the difference, δ, between the computed and experimental ω_{01}(OD) values is also reported. From these values, it appears that, whereas HF always largely overestimates with respect to experiment (the usual electron correlation error), δ is negative for all considered DFT methods. For LDA, it is as large as −857 cm^{-1}, showing that LDA is inadequate for describing H-bonded systems. PW91 is much better, even if the maximum error is close to −400 cm^{-1}. Only B3LYP gives results in remarkable agreement with experiment, with a maximum error of 120 cm^{-1}. The portion of exact HF exchange contained in the definition of the B3 exchange part has a beneficial effect in reducing the self-interaction error which is particularly severe for H-containing bonds, causing too long OH bonds and too low vibrational frequencies.

Such a correlation between geometry and vibrational frequency for the H-bonded systems indeed exists, as shown by Figure 4, where the difference between the computed and experimental OH1···O2 and OH2···O1 intermolecular distances is reported versus δ, the error in the ω_{01} frequency. The correlation is essentially linear, with the data for all DFT methods aligned along a common line and B3LYP showing the best behavior among the considered Hamiltonians.

3.3. Effects of Deuteration on the Coupling between OH Modes of the Same Family. In the previous section, the total symmetric OH1 and OH2 modes have been analyzed considering the simultaneous stretching of the four OH involved bonds within each family. To investigate the role of the mechanical coupling within the OH bonds belonging to the same family (OH1 or OH2), a series of isotopic substitution with deuterium replacing gradually all but one hydrogen atom has been carried out. A symmetric analysis has been carried out by starting from a fully deuterated system and gradually replacing all deuterium atoms but one with hydrogen. Table 5 shows the B3LYP results: within the OH1 family, the initial ω_h(OH1) frequency *decreases* by 17 cm^{-1} when only one isolated OH1 group is present in the unit cell. On the contrary, within the OH2 family, the initial ω_h(OH2) frequency *increases* by 33 cm^{-1} upon deuteration of the remaining hydrogen atoms. The same trend

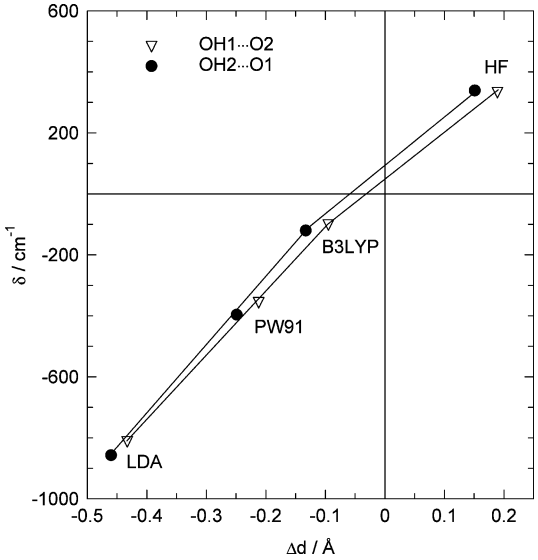

Figure 4. Correlation for β-$Be(OH)_2$ between Δd, the difference between the calculated and experimental OH1···O2 and OH2···O1 distances, and δ, the difference between the calculated and experimental ω_{01} OD1 and OD2 frequencies.

TABLE 5: B3LYP Harmonic OH (OD) Frequency of the Total Symmetric OH1 and OH2 Modes as a Function of the Deuteration for β-$Be(OH)_2$[a]

OH1 family	frequency	OD1 family	frequency
$(\mathbf{H1})_4\,(H2)_4$	3585	$(\mathbf{D1})_4\,(D2)_4$	2618
$(\mathbf{H1})_4\,(D2)_4$	3564	$(\mathbf{D1})_4\,(H2)_4$	2603
$(\mathbf{H1})(D1)_3\,(D2)_4$	3569	$(\mathbf{D1})(H1)_3\,(H2)_4$	2606
OH2 family	**frequency**	**OD2 family**	**frequency**
$(H1)_4\,(\mathbf{H2})_4$	3501	$(D1)_4\,(\mathbf{D2})_4$	2561
$(D1)_4\,(\mathbf{H2})_4$	3525	$(H1)_4\,(\mathbf{D2})_4$	2574
$(D1)_4\,(\mathbf{H2})(D2)_3$	3533	$(H1)_4\,(\mathbf{D2})(\mathbf{H2})_3$	2580

[a] All data are in inverted centimeters.

is computed for the fully deuterated system, with values of 12 and 20 cm^{-1} for OD1 and OD2, respectively (see Table 5). Careful inspection of the data in Table 5 also reveals that the mechanical coupling is more relevant between different families of OH groups (23 and 24 cm^{-1} for OH1 and OH2, respectively) than within the same OH family (6 and 9 cm^{-1} for OH1 and OH2, respectively).

4. Conclusions

The present work has shown that, among the four considered Hamiltonians, namely, HF, LDA, PW91, and B3LYP, only the latter is in remarkable agreement with both the experimental structural and OH vibrational data of $Mg(OH)_2$ and β-$Be(OH)_2$ crystals. In particular, the agreement is very good for $Mg(OH)_2$, where no H-bonding is present in the structure, the predicted ω_{01}(OH) frequency being within 10 cm^{-1} of the experimental value. It turns out that the splitting between the symmetric and antisymmetric OH stretching modes is controlled by the interlayer distance.

For β-$Be(OH)_2$, where infinite networks of H-bonds of intermediate strength exist, the OH stretching frequencies give rise to eight distinct modes at Γ point, which are grouped into two families, involving mainly OH1 and OH2 modes. For the two OH symmetric modes, a full anharmonic analysis has been performed. B3LYP slightly underestimates the ω_{01}(OH) frequencies, the difference being around 120 cm^{-1}.

Although HF always overestimated the ω_{01}(OH) frequencies, LDA grossly underestimated all of them, particularly so for OH frequencies involved in H-bonds in which the deviation from the experiment was as large as -850 cm^{-1}, indicating that this level of theory is not adequate for treating crystalline H-bonded systems. The PW91 Hamiltonian, which is commonly adopted in a variety of widely used plane-wave-based computer codes, performs much better than LDA, even if the error in the ω_{01}-(OH) frequencies for the β-$Be(OH)_2$ system, ~ -400 cm^{-1}, remains too large for accurate predictions of the stretching frequencies of the OH groups involved in H-bonds.

Acknowledgment. Computer support from the CINECA supercomputing center is kindly acknowledged. This work was supported in part by the 'Centre National de la Recherche Scientifique' (CNRS) and the 'Ministère de l'Enseignement Supérieure et de la Recherche' (MESR). Some of the calculations were carried out on the IBM/SP3 computer at the 'Centre Informatique National de l'Enseignement Supérieur' (CINES). We thank the scientific council of IDRIS for their support for this project.

References and Notes

(1) Koch, W.; Holthausen, M. C. *A Chemist's Guide to Density Functional Theory*; Wiley-VCH Verlag GmbH: Weinheim, Germany, 2000.
(2) Perdew, J. P.; Wang, Y. *Phys. Rev. B* **1986**, *33*, 8800.
(3) Perdew, J. P.; Wang, Y. *Phys. Rev. B* **1989**, *40*, 3399.
(4) Perdew, J. P. *Electronic Structure of Solids*; Akademie Verlag: Berlin, 1991.
(5) Perdew, J. P.; Wang, Y. *Phys. Rev. B* **1992**, *45*, 13244.
(6) Becke, A. D. *J. Chem. Phys.* **1993**, *98*, 5648.
(7) Civalleri, B.; Ugliengo, P. *J. Phys. Chem. B* **2000**, *104*, 9491.
(8) Civalleri, B.; Garrone, E.; Ugliengo, P. *THEOCHEM* **1997**, *419*, 227.
(9) Pascale, F.; Zicovich-Wilson, C. M.; Gejo, F. L.; Civalleri, B.; Orlando, R.; Dovesi, R. *J. Comput. Chem.* **2004**, *25*, 888.
(10) Catti, M.; Ferraris, G.; Hull, S.; Pavese, A. *Phys. Chem. Miner.* **1995**, *22*, 200.
(11) Stahl, R.; Jung, C.; Lutz, H. D.; Kockelmann, W.; Jacobs, H. *Z. Anorg. Allg. Chem.* **1998**, *624*, 1130.
(12) Jacobs, H. Private communication.
(13) Lutz, H. D.; Jung, C.; Mortel, R.; Jacobs, H.; Stahl, R. *Spectrochim. Acta, Part A* **1998**, *54*, 893.
(14) Saunders, V. R.; Dovesi, R.; Roetti, C.; Orlando, R.; Zicovich-Wilson, C. M.; Harrison, N. M.; Doll, K.; Civalleri, B.; Bush, I. J.; D'Arco, P.; Llunell, M. *CRYSTAL03 User's Manual*; University of Torino: Torino, Italy, 2003.
(15) Zicovich-Wilson, C. M.; Pascale, F.; Catti, M. *LoptCGBerny* (a Perl script for crystal structure optimization using CRYSTAL03); unpublished, 2004.
(16) Doll, K.; Harrison, N. M.; Saunders: V. *Int. J. Quantum Chem.* **2000**, *82*, 1.
(17) Doll, K. *Comput. Phys. Commun.* **2001**, *137*, 74.
(18) Schlegel, H. B. *J. Comput. Chem.* **1982**, *3*, 214.
(19) Dirac, P. A. M. *Proc. Cambridge Philos. Soc.* **1930**, *26*, 376.
(20) Vosko, S. H.; Wilk, L.; Nusair, M. *Can. J. Phys.* **1980**, *58*, 1200.
(21) Lee, C.; Yang, W.; Parr, R. G. *Phys. Rev. B* **1988**, *37*, 785.
(22) Harrison, N. M.; Saunders, V. R. *J. Phys.: Condens. Matter* **1992**, *4*, 3873.
(23) Harrison, N. M.; McCarthy, M. I. *Phys. Rev. B* **1994**, *49*, 8574.
(24) Dovesi, R.; Roetti, C.; Freyria-Fava, C.; Aprà, E.; Saunders, V. R.; Harrison, N. M. *Philos. Trans. R. Soc. London, Ser. A* **1992**, *341*, 203.
(25) Lichanot, A.; Chaillet, M.; Larrieu, C.; Dovesi, R.; Pisani, C. *Chem. Phys.* **1992**, *164*, 383.
(26) Merawa, M.; Labeguerie, P.; Ugliengo, P.; Doll, K.; Dovesi, R. *Chem. Phys. Lett.* **2004**, *387*, 453.
(27) Merawa, M.; Civalleri, B.; Ugliengo, P.; Noel, Y.; Lichanot, A. *J. Chem. Phys.* **2003**, *119*, 1045.
(28) Lindberg, B. *J. Chem. Phys.* **1988**, *88*, 3805.
(29) Ugliengo, P. *ANHARM* (a program to solve the monodimensional nuclear Schroedinger equation); unpublished, 1989.
(30) Weckler, B.; Lutz, H. D. *Spectrochim. Acta, Part A* **1996**, *52*, 1507.
(31) Mitra, S. S. *Solid State Phys.* **1962**, *13*, 1.
(32) Martens, R.; Freund, F. *Phys. Status Solidi A* **1976**, *37*, 97.
(33) Freund, F. *Proton Conductors: Solids, Membranes and Gels—Materials and Devices*; Cambridge University Press: New York, 1992.
(34) Engstrom, H.; Bates, J. B.; Boatner, L. A. *J. Chem. Phys.* **1980**, *73*, 1073.
(35) Berglund, B.; Lindgren, J.; Tegenfeldt, J. *J. Mol. Struct.* **1978**, *43*, 169.
(36) Zicovich-Wilson, C. M.; Dovesi, R.; Pascale, F. Manuscript in preparation.